



## Biomass gasification in a circulating fluidized bed

X.T. Li<sup>a</sup>, J.R. Grace<sup>a,\*</sup>, C.J. Lim<sup>a</sup>, A.P. Watkinson<sup>a</sup>, H.P. Chen<sup>b</sup>, J.R. Kim<sup>c</sup>

<sup>a</sup>*Department of Chemical and Biological Engineering, The University of British Columbia, 2216 Main Mall, Vancouver, Canada V6T 1Z4*

<sup>b</sup>*National Laboratory of Coal Combustion, Huazhong University of Science and Technology, Wuhan 430074, China*

<sup>c</sup>*Hyundai Industrial Research Institute, Hyundai Heavy Ind. Co., Ltd., 1, Cheonha-Dong, Dong-Ku, Ulsan, South Korea 682-792*

Received 10 October 2002; received in revised form 17 April 2003; accepted 28 April 2003

### Abstract

This paper presents the results from biomass gasification tests in a pilot-scale (6.5-m tall  $\times$  0.1-m diameter) air-blown circulating fluidized bed gasifier, and compares them with model predictions. The operating temperature was maintained in the range 700–850°C, while the sawdust feed rate varied from 16 to 45 kg/h. Temperature, air ratio, suspension density, fly ash re-injection and steam injection were found to influence the composition and heating value of the product gas. Tar yield from the biomass gasification decreased exponentially with increasing operating temperature for the range studied. A non-stoichiometric equilibrium model based on direct minimization of Gibbs free energy was developed to predict the performance of the gasifier. Experimental evidence indicated that the pilot gasifier deviated from chemical equilibrium due to kinetic limitations. A phenomenological model adapted from the pure equilibrium model, incorporating experimental results regarding unconverted carbon and methane to account for non-equilibrium factors, predicts product gas compositions, heating value and cold gas efficiency in good agreement with the experimental data.

© 2003 Elsevier Ltd. All rights reserved.

*Keywords:* Biomass gasification; Modelling; Elemental availability; Circulating fluidized bed; Tar

### 1. Introduction

Biomass gasification produces fuel gas or synthesis gas through the chemical conversion of biomass, usually involving partial oxidation of the feedstock in a reducing atmosphere in the presence of air, oxygen and/or steam. Air-blown processes produce low calorific value gases with a typical higher heating value (HHV) of 4–7 MJ/Nm<sup>3</sup>, while oxygen- and steam-blown processes result in gases with a HHV

of 10–18 MJ/Nm<sup>3</sup> [1]. According to a recent survey [2], there are nearly 100 biomass gasification and/or pyrolysis installations in Europe and North America.

Various types of gasifiers have been explored for biomass. Updraft moving-bed gasifiers suffer from high tar yields in the product gas [3]. The inability to maintain uniform radial temperature profiles and to avoid local slagging problems makes the moving bed unsuitable for large installations [4]. Fluidized beds now find wide application in biomass gasification [5–8]. However, due to their high degree of solids mixing as well as particle entrainment, a single fluidized bed cannot achieve high solids conversion. The circulating fluidized bed (CFB) is a natural extension of the bubbling bed concept, with cyclones or other separators

\* Corresponding author. Tel.: +1-604-822-3121; fax: +1-604-822-6003.

E-mail address: [jgrace@chml.ubc.ca](mailto:jgrace@chml.ubc.ca) (J.R. Grace).

### Nomenclature

$a$	air ratio, defined as ratio of actual air supply to stoichiometric air requirement, dimensionless
$b$	element abundance vector, dimensionless
$b_0$	initial element abundance vector, dimensionless
$b^*$	element abundance vector modified with kinetic carbon conversion, dimensionless
$C$	carbon conversion, %
$C_{fa}$	carbon content in fly ash, % of mass
$C_f$	carbon content in fuel, dry basis, %
$E_1$	cold-gas efficiency excluding tars, %
$E_2$	cold-gas efficiency including tars, %
$F$	ratio of carbon in re-injected fly ash to carbon introduced with fuel, dimensionless
$g$	acceleration of gravity, $9.81 \text{ m/s}^2$
GCV	gross calorific value of fuel, MJ/kg
$\Delta H_{298}^0$	heat of reaction at thermodynamic standard state, kJ/mol
HHV	higher heating value of product gas, MJ/Nm <sup>3</sup> , or tars, MJ/kg
$\Delta h$	height of a section of the riser, m
$K$	total number of components
$L$	total number of feed streams
$M$	moisture content of feed, kg/kg (dry basis)
$(m)$	number of iterations, dimensionless
$\dot{m}$	feed rate, kg/h
$n$	moles of a given element or species, mol
$N$	total number of species involved in the system
$\Delta P$	pressure difference, kPa
$T$	thermodynamic temperature, K
$T_3$	characteristic operating temperature measured 3.95 m above primary air inlet, °C

$T_{eq}^0$	equilibrium temperature from best fit to experimental data, K
$v_g$	gas yield based on unit mass of feed, Nm <sup>3</sup> /kg
$y$	number of moles, mol
$y_t$	tar yield, kg/kg-fuel

### Greek letters

$\beta$	elemental availability, or fractional achievement of equilibrium, dimensionless
$\beta_C$	availability of carbon, dimensionless
$\beta_{C,1}$	fraction of carbon converted into gaseous species, dimensionless
$\beta_{C,2}$	fraction of carbon converted into methane, dimensionless
$\beta_H$	availability of hydrogen, dimensionless
$\bar{\epsilon}$	suspension voidage
$\pi$	total number of phases in system
$\rho$	density, kg/m <sup>3</sup>

### Subscripts

0	initial
C, H, N, O, S	carbon, hydrogen, nitrogen, oxygen, sulphur
eq	equilibrium model prediction
f	biomass feed
fa	fly ash
g	product gas
meas	measurement data
p	particles
susp	suspension
t	tars

### Superscripts

*	modified value
o	thermodynamic standard state

employed to capture and recycle solids in order to extend the solids residence time. The riser of a CFB gasifier operates in either the turbulent or fast fluidization flow regime. CFB gasification is now undergoing rapid

commercialization for biomass. Fundamental and pilot studies are, nevertheless, required for scale-up, as well as to fill gaps in understanding the underlying principles.

Several different types of models [9–13] have been developed for gasification systems—kinetic, equilibrium, and other. Unlike kinetic models that predict the progress and product composition at different positions along a reactor, an equilibrium model predicts the maximum achievable yield of a desired product from a reacting system. It also provides a useful design aid in evaluating the limiting possible behaviour of a complex reacting system which is difficult or unsafe to reproduce experimentally or in commercial operation.

The objective of this study is to provide practical data and a theoretical perspective for scale-up from both pilot-scale experimental study and mathematical modelling. An experimental study was completed on a circulating fluidized bed gasifier to examine the effects of operating parameters on the gas composition, gasification efficiency and tar yield. The modelling work started with a non-stoichiometric equilibrium model based on free energy minimization to predict gasifier performance under ideal equilibrium conditions. The present study not only gives experimental evidence that real gasifiers deviate from chemical equilibrium in a number of ways, but also provides a phenomenological approach to correct the model by introducing an elemental availability function which corrects for non-equilibrium of certain components.

## 2. Experimental study

### 2.1. Experimental set-up and method

A schematic diagram of the pilot CFB gasifier used in the experiments appears in Fig. 1. The gasifier employs a riser 6.5 m high and 0.10 m in diameter, a high-temperature cyclone for solids recycle and ceramic fibre filter unit for gas cleaning. Air was supplied as the oxidant and fluidizing agent after passing through a start-up burner near the bottom of the riser. Hot gas leaving the burner and pre-heated air were mixed to preheat the bed and, if needed, to maintain the suspension temperature at the desired level. The temperatures of both the primary and secondary air could be varied by adjusting the total air supply and the fraction of each stream. The start-up burner preheated the gasifier to 400–550°C before coal or biomass fuel could be fed to the riser to further raise the temperature to the desired level.

The system was then switched to the gasification mode.

Feed particles underwent moisture evaporation, pyrolysis and char gasification primarily in the riser. The fast fluidization flow regime was maintained at the operating temperature, with a typical superficial velocity between 4 and 10 m/s, corresponding to an air flow of 40–65 Nm<sup>3</sup>/h, and a solids feedrate of 16–45 kg/h for typical sawdust. The solids throughput was estimated to be 0.7–2.0 kg/m<sup>2</sup> s. Coarser particles in the gas were captured by a high-temperature cyclone immediately downstream of the riser. The solids captured in the cyclone were recycled to the bottom of the riser through an air-driven loop seal. Hot gas leaving the cyclone at a temperature of 600–800°C was cooled by a two-stage water-jacketed heat exchanger and a single-stage air preheater before entering the filter unit.

The gasifier employs two independent feed systems, one for the main fuel (biomass) and the other for auxiliary fuel (coal), used during start-up. The biomass feed system consisted of two sealed hoppers, each of volume 0.3 m<sup>3</sup>, a rotary valve with a variable-speed DC motor and controller, and a screw with a tapered pitch and sleeve diameter to allow 10% compaction of the sawdust volume to facilitate feeding. The upper hopper could be refilled while the lower hopper is in service. A 0.2 m diameter pinch valve isolated the upper hopper from the working pressure in the riser, thus allowing safe refilling without interrupting the operation of the CFB reactor. The coal feed system (not shown in Fig. 1) employed a hopper, a rotary valve and a 10 mm dia. pneumatic conveying line connected with a water-cooled injector 950 mm above the primary air inlet.

The steam injection system supplied 5 bar saturated steam. The steam flow rate was measured with an in-line annubar steam meter, calibrated by weighing condensate water over a known time interval.

Process data, such as local temperatures and pressures, were logged into a computer. The thermocouple readings in the mid-section of the riser ( $T_3$ ) are taken as the characteristic operating temperatures unless specified otherwise. Gas sampling ports were located near the inlet of the heat exchanger. Gas samples were taken on average every 20 min and analysed for H<sub>2</sub>, CO, CO<sub>2</sub>, CH<sub>4</sub>, N<sub>2</sub> and O<sub>2</sub> using a Shimadzu gas chromatograph with a thermal conductivity detector and a Supelco Carboxen-1000

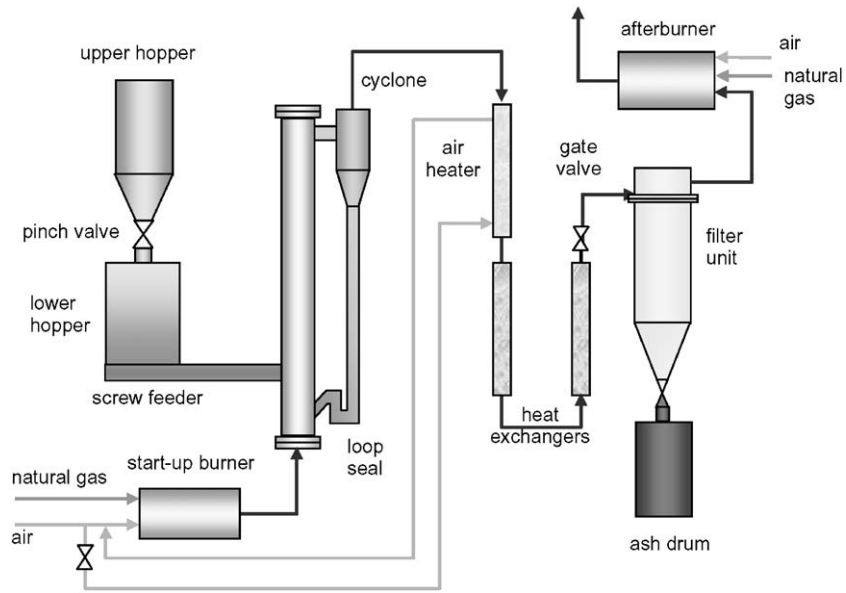


Fig. 1. Schematic diagram of the CFB gasifier.

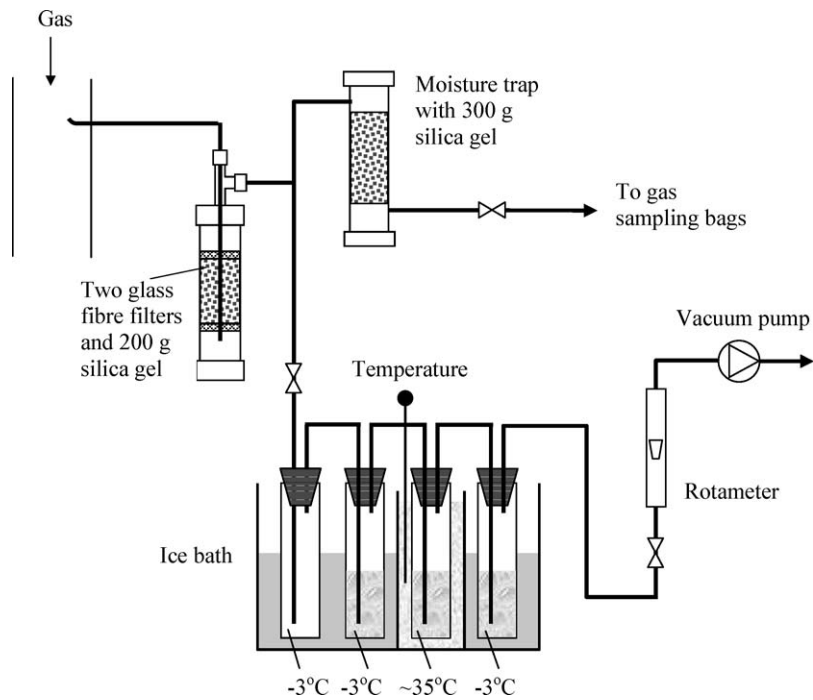


Fig. 2. Tar sampling train: The first empty bottle acts as a condenser. The three filled ones are tar impingers, with acetone as solvent. Temperature varies from  $-3^{\circ}\text{C}$  to about  $35^{\circ}\text{C}$  in the three impingers.

Table 1  
Ultimate analysis of test fuels<sup>a</sup>

Fuel type		Cypress	Hemlock	SPF <sup>b</sup>	Cedar	PS <sup>c</sup>	Mixed	Average
Carbon	wt%	51.6	51.8	50.4	52.3	49.1	48.9	50.9
Hydrogen	wt%	6.20	6.20	6.25	6.11	7.26	7.86	6.60
Oxygen	wt%	40.4	40.6	41.6	39.9	39.5	40.3	40.5
Nitrogen	wt%	0.65	0.60	0.62	0.52	0.25	0.21	0.51
Sulphur	wt%	0.46	0.38	0.34	0.39	0.50	0.07	0.34
Ash	wt%	0.70	0.40	0.70	0.79	3.34	2.69	1.14
Moisture content	wt%	9.7–22.0	8.8–15.0	10.0	10.6	10.1	4.2–6.7	15.0
Higher heating value	MJ/kg	20.3	20.3	19.8	20.4	21.1	21.7	20.6
Higher heating value	kcal/kg	4840	4850	4720	4880	5030	5170	4920
Stoichiometric air	Nm <sup>3</sup> /kg	5.36	5.36	5.20	5.40	5.46	5.56	5.39
Dry bulk density	kg/m <sup>3</sup>	136	128	119	151	347	465	220
Mean particle diameter	mm	1.49	0.92	0.82	0.67	0.38	0.43	0.79

<sup>a</sup>All ultimate analyses, heating values and stoichiometric air volumes are on a dry basis.

<sup>b</sup>SPF = spruce, pine and fir mixed sawdust.

<sup>c</sup>PS = 50 wt% pine bark 50 wt% spruce whitewood mix.

column. The gas and tar sampling device is shown in Fig. 2. Tar yield was measured by in-line tar sampling using a sampling train simplified from the Tar Protocol [14], together with post-test direct tar collection from the stack. The tar sampling train employed four 250 ml impingers, with acetone as the solvent, working alternately at  $-3^{\circ}\text{C}$  and room temperature (about  $35^{\circ}\text{C}$  in the sampling area) in order to reduce tar fog by forming larger droplets at room temperature that are easier to capture in the next impinger.

Six sawdust species were tested; their ultimate analyses and other relevant properties appear in Table 1. Each sawdust was dried before being charged to the hoppers. Bed ash collected from a previous run was used as the starting bed material for each new run, with silica sand making up for loss of solids. In some runs, fly ash collected from the outlet product stream was pneumatically re-injected into the bottom of the riser. The air used for re-injecting fly ash was included when calculating the air ratio. The carbon content of the bed materials and re-injected fly ash was accounted for in the overall mass and energy balance. In the last two runs, a nickel-based catalyst (C11-9 LDP, Süd-Chemie) was used for tar removal and methane reforming. Its particle density is  $2820\text{ kg/m}^3$ . In each of these two runs, a batch of about 11–14 kg of catalyst, crushed and screened to 0.25–1.7 mm in diameter, was added to the riser by pneumatic conveying immediately prior to switching the system to the gasification mode.

Fifteen test runs were conducted on the CFB gasifier, each with particular objectives, contributing to a detailed parametric study of the effects of operating temperature, air ratio, suspension density, steam injection, fly ash re-injection, secondary air rate and catalyst addition. The operating pressure in the system was maintained at  $\sim 1.05$  bar, slightly higher than atmospheric, except for the first run, in which the pressure was 1.65 bar. The influences of the sawdust species and moisture content were examined by comparing results from different fuels.

A number of operating parameters can be used to characterize gasification processes. The air ratio,  $a$ , defined as the ratio of the actual air supply to the stoichiometric air required for complete combustion, is one such measure. We also use the O/C molar ratio where steam or ash re-injection is involved. Since sawdust has a high oxygen content, the minimum O/C ratio is about 0.6, corresponding to air-free pyrolysis conditions. The gas heating value is usually given as the HHV of the dry product gas in  $\text{MJ/Nm}^3$ . The tar yield is expressed as the mass of tar per unit volume of raw gas, in  $\text{g/Nm}^3$ . An alternative definition [15] is the mass of tar produced per unit mass of dry biomass feed.

## 2.2. Temperature and gas composition profiles

Fig. 3 shows radial and axial temperature distributions in the riser. The radial temperature profile for

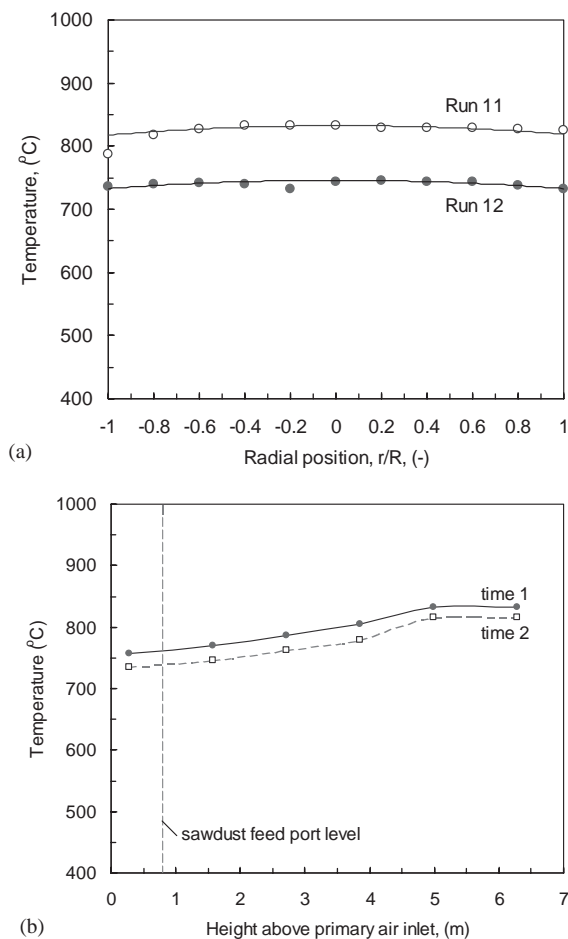


Fig. 3. Measured temperature profiles in the CFB gasifier. (a) Radial profiles:  $\circ$ —air ratio  $a=0.325$ ,  $T_3=789^\circ\text{C}$ ;  $\bullet$ — $a=0.23$ ,  $T_3=701^\circ\text{C}$ ; (b) axial profiles, measured from Run 11 at  $r/R=1$ ,  $a=0.325$ ,  $T_3=789^\circ\text{C}$ . For experimental operating conditions, see Table 2.

Run 11 shown in Fig. 3(a) indicates that there could be as much as a  $45^\circ\text{C}$  difference between the core and wall region of the riser. Later measurements from Run 12 from the opposite side, with the thermocouple tip withdrawn 2 mm from the wall, showed improved symmetry and less than a  $15^\circ\text{C}$  centre-to-wall temperature difference. This temperature uniformity indicates extensive radial mixing and radial heat transfer in the riser, facilitating both homogeneous and heterogeneous reactions.

The axial profile of suspension temperature at constant  $r/R=1$  is shown in Fig. 3(b). The tempera-

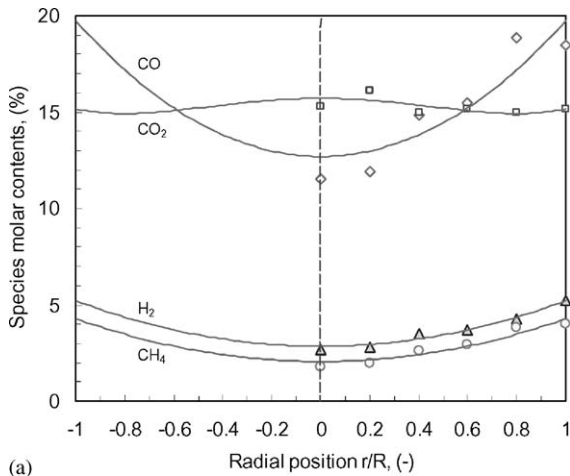
ture difference across most of the riser height was less than  $100^\circ\text{C}$ , consistent with normal CFB reactors. The measured temperature at the bottom of the riser was  $600\text{--}700^\circ\text{C}$  for all test runs. The coarser particles settled at the bottom and cooled there. However, intense solids recycle minimized the temperature gradient.

In a circulating fluidized bed operating in the fast fluidization flow regime, particles tend to migrate outwards toward the wall, driven by fluid–particle interactions and boundary effects, and descend along the wall, while dilute upflow is maintained in the inner core [16]. As a result of the higher concentration of particles in the wall region, there is a reducing region there, with augmented  $\text{CH}_4$ ,  $\text{H}_2$  and  $\text{CO}$  concentrations as shown in Fig. 4(a).

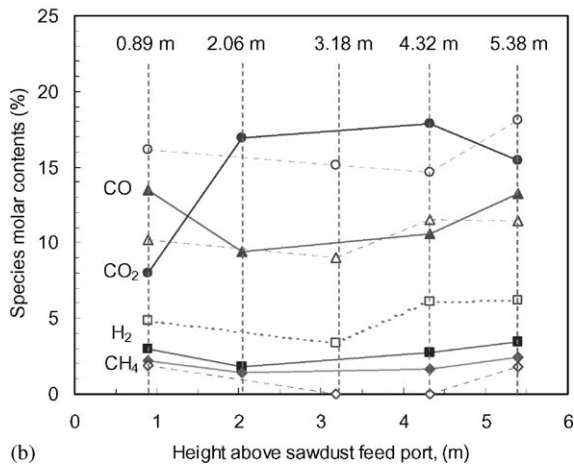
The axial gas composition profile is plotted in Fig. 4(b). The lower part of the riser mainly provided pyrolysis of returning particles and evaporation of moisture from fresh particles. For  $a=0.38$ , a major rise in  $\text{CO}_2$  content was observed over the 0.9–2.0 m height interval where the partial oxidation of pyrolysis products resulted in a simultaneous decrease in the concentrations of  $\text{CO}$  and other combustible species. Gasification of char continued along the remainder of the riser, raising the  $\text{CO}$  and  $\text{H}_2$  contents again. Although a cross-over of  $\text{CO}$  and  $\text{CO}_2$  contents occurred for  $a=0.38$ , this crossover was not repeated for higher air ratio ( $a=0.46$ ). The concentration of  $\text{CH}_4$  never approached its equilibrium level due to the limited gas residence time in the riser. The measured  $\text{N}_2$  content (not shown) decreased monotonically along the riser height, indicating increasing conversion of carbonaceous species.

### 2.3. Effects of air ratio and O/C molar ratio

Fig. 5 portrays the changes in the concentrations of different species vs. air ratio, with the short straight lines suggesting general trends rather than true linear relationships. The concentrations of  $\text{CO}_2$  and  $\text{H}_2\text{O}$  would be expected to increase with increasing air ratio, while the concentrations of reducing species, such as  $\text{CO}$ ,  $\text{H}_2$  and  $\text{CH}_4$ , decrease. Notwithstanding the improved carbon conversion at higher air ratios, the total fraction of combustible species decreases with increasing air ratio, since the increase in the inert nitrogen far exceeds the gains in wood-borne species.



(a)



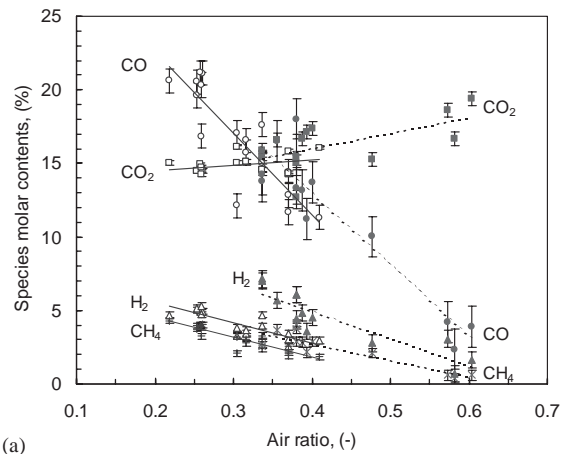
(b)

Fig. 4. Radial and axial gas composition profiles: (a) radial profiles. Run 7,  $T_3 = 815^\circ\text{C}$ ,  $a = 0.45$ . Gas samples taken 5.09 m above the primary air inlet; (b) axial profiles. Solid lines and closed points: Run 3,  $a = 0.38$ ,  $T_3 = 750^\circ\text{C}$ , Moisture content of sawdust  $M = 10.5\%$ ; dashed lines and open points: Run 15,  $a = 0.46$ ,  $T_3 = 805^\circ\text{C}$ ,  $M = 4.2\%$ . Gas samples taken at  $r/R = 1$ . See Table 2 for operating conditions.

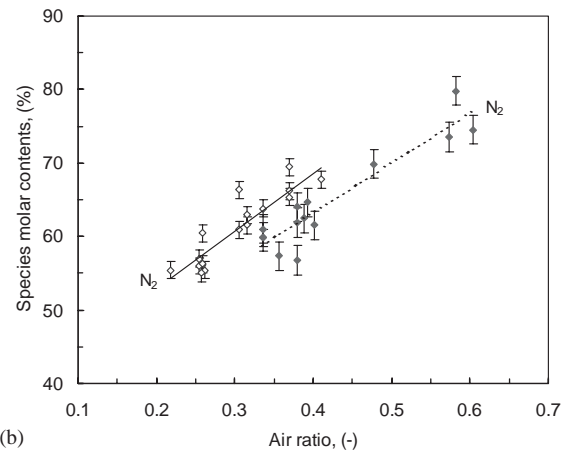
The dry gas higher heating value at the standard state of 101.3 kPa and 273 K can be estimated from the gas composition by

$$\text{HHV} = (12.75[\text{H}_2] + 12.63[\text{CO}] + 39.82[\text{CH}_4] + 63.43[\text{C}_2\text{H}_4] + \dots)/100, \quad (1)$$

where the species contents are given in mol%, and their heats of combustion, in  $\text{MJ}/\text{Nm}^3$ . This equation is based on heat of combustion data [17], assuming



(a)



(b)

Fig. 5. Effect of air ratio on instantaneous values of gas composition: fuel moisture  $M = 6.6\text{--}22.0\%$ . Solid lines and symbols for riser temperatures  $T_3 = 700 \pm 10^\circ\text{C}$ , dashed lines and open symbols for  $T_3 = 820 \pm 10^\circ\text{C}$ . Symbols:  $+/\times = \text{CH}_4$ ,  $\triangle/\blacktriangle = \text{H}_2$ ,  $\circ/\bullet = \text{CO}$ ,  $\square/\blacksquare = \text{CO}_2$ ,  $\diamond/\blacklozenge = \text{N}_2$ .

ideal-gas behaviour for the gaseous species. Although ethylene is listed in Eq. (1), the concentrations of ethylene and higher hydrocarbons are often too low to be detected. Since gas heating value can be significantly altered by the presence of even small percentages of these hydrocarbons, accurate measurement of them is crucial when the gasifier operates at temperatures below  $700^\circ\text{C}$  or at elevated pressure.

Fig. 6 shows how the time-mean dry gas heating value varies with air ratio over the entire range tested. It is seen that the time-mean gas heating value

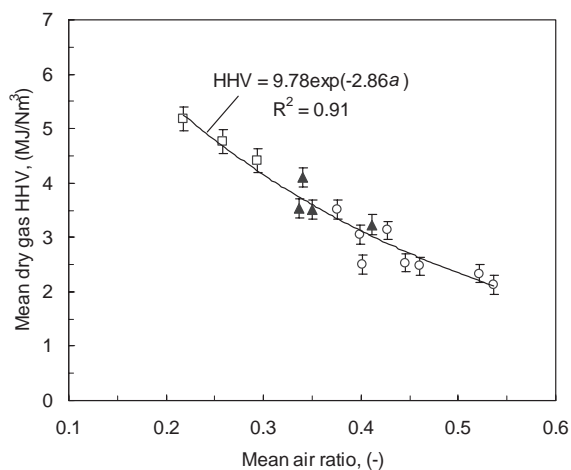


Fig. 6. Effect of air ratio and feed rate on mean dry gas heating value:  $T = 700\text{--}850^\circ\text{C}$ ,  $M = 6.6\text{--}15.0\%$ . Data from test runs using six sawdust species; feed rates:  $\circ$ —16–27 kg/h;  $\blacktriangle$ —31–35 kg/h;  $\square$ —40–49 kg/h.

can be approximated as an exponential function of the air ratio

$$\text{HHV} = 9.78 \exp(-2.86a) \quad (0.22 \leq a \leq 0.54). \quad (2)$$

The correlation coefficient for this relationship is  $R^2 = 0.91$ . The standard error (SE) of the gas heating value is shown by error bars, suggesting 7–8% of the mean value. More scatter was observed in the instantaneous gas heating value data. For a sample set of instantaneous gas HHV data representing a typical air ratio of 0.33, the standard deviation range corresponding to a 95% confidence interval (CI) is  $3.87 \pm 0.59 \text{ MJ/Nm}^3$ . For comparison, different ranges of feedrate are denoted by different symbols in Fig. 6. It appears that feed rate has no significant influence on the trend for the feedrate range tested. However, the methane content in the product gas was high ( $> 4\%$ ) when the feedrate exceeded 40 kg/h, suggesting that the system was reaching its throughput limit as the gas residence time became inadequate for cracking of hydrocarbons.

The use of the O/C molar ratio is clearly preferred to the air ratio for steam- or  $\text{CO}_2$ -blown processes. In view of this, an alternative correlation for the measured dry gas heating value was obtained:

$$\text{HHV} = 34.38 \exp(-1.37[\text{O/C}]) \quad (1.1 \leq \text{O/C} \leq 2.1). \quad (3)$$

The correlation coefficient of this equation is  $R^2 = 0.86$ . The gas heating value could equally be correlated versus the  $\text{O}/[\text{C} + \text{H}]$  or  $\text{O}/[\text{C} + \text{H}/4]$  molar ratio, when the molar abundance of hydrogen in the system is comparable to that of carbon.

Three molar ratios are commonly used to characterize the gas composition:  $\text{CO}/\text{CO}_2$ ,  $\text{H}_2/\text{CO}$  and  $\text{CH}_4/\text{H}_2$ . The O/C molar ratio varied between 1.1 and 2.1 for most cases tested. As more oxygen is supplied, more  $\text{CO}_2$  is formed, causing the  $\text{CO}/\text{CO}_2$  ratio to decrease. Since the  $\text{H}_2$  concentration in the raw gas is mainly determined by the water–gas shift reaction, it is less sensitive to the O/C ratio than is the  $\text{CH}_4$  concentration. The  $\text{H}_2/\text{CO}$  molar ratio increases slightly with increasing O/C, while the  $\text{CH}_4/\text{H}_2$  molar ratio decreases more sharply. It was found that air-blown gasification of biomass usually resulted in a  $\text{H}_2/\text{CO}$  molar ratio less than 1, as in a previous study [18] in a bubbling fluidized bed gasifier. Injection of steam as gasifying agent increases the  $\text{H}_2/\text{CO}$  molar ratio because moisture promotes both steam gasification and the CO-shift reaction.

Modelling work [19] indicates that the equilibrium methane concentration in the fuel gas is less than 0.1% by volume for the temperature and pressure ranges tested. This suggests that the high  $\text{CH}_4/\text{H}_2$  ratio of the product gas (0.6–0.8) from the pilot plant tests was not due to methanation. Instead, it resulted from incomplete thermal cracking of pyrolysis products and incomplete reforming reactions.

#### 2.4. Effect of operating temperature

Operating temperature plays an important role in biomass gasification. Fig. 7 shows that the gas heating value increases slightly with increasing temperature for constant values of the air ratio. This is because of improved carbon conversion at higher temperatures. As shown in Fig. 7, the increase in gas HHV is approximately 10% for an increase in operating temperature from  $700^\circ\text{C}$  to  $800^\circ\text{C}$ . This increase of gas heating value with increasing temperature indicates that the gasifier can benefit from better thermal insulation and from air preheating. System pressure showed little effect on gas composition for the limited range tested (1.0–1.65 bar).

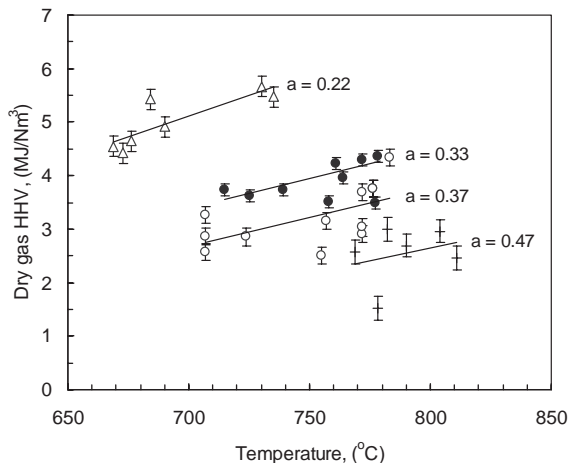


Fig. 7. Effect of operating temperature on dry gas heating value.  $M = 6.6\text{--}15.0\%$ . Air ratios for each group of data points are given.

### 2.5. Effect of secondary air

Secondary air was found to have only a small effect on the gas composition. A previous study [20] showed that secondary air contributed to tar removal, but at the expense of lowering the gas heating value, with a 14% decrease in the gas heating value as the secondary air fraction increased from zero to 20%. The mechanism proposed for tar removal due to addition of secondary air [20] is the formation of local high-temperature zones where thermal cracking of tar is promoted.

Experimental results obtained in this work indicate that the gas heating value dropped from an average of  $4.20 \text{ MJ/Nm}^3$  for no secondary air to  $4.02 \text{ MJ/Nm}^3$  for 14.3% secondary air at constant total air flow, less than a 5% decrease. This decrease was less pronounced than reported previously [20]. However, in the earlier work, there appeared to be an increase in total air supply as the secondary air level increased. Secondary air caused only a slight change in gas composition for the range of conditions investigated in this work.

### 2.6. Effect of suspension density

In most CFB systems the solids gravity term is an order of magnitude greater than terms due to wall friction, acceleration and gas gravity. The pressure drop

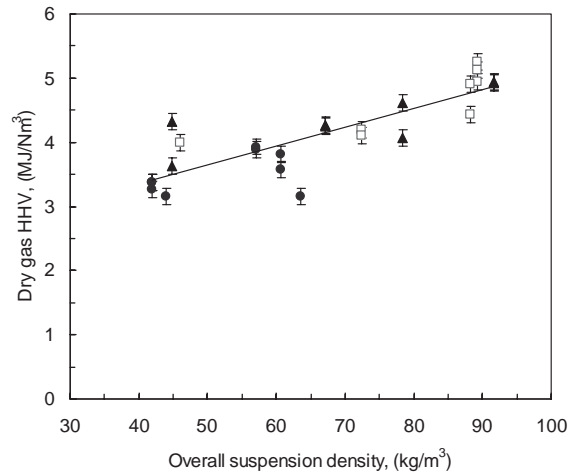


Fig. 8. Effect of suspension density on gas heating value: ●—Hemlock sawdust,  $a = 0.337$ ,  $T = 715\text{--}780^\circ\text{C}$ ,  $M = 14.7\%$ ; □—Pine and spruce mix,  $a = 0.218$ ,  $T = 676\text{--}735^\circ\text{C}$ ,  $M = 10.1\%$ ; ▲—Mixed sawdust,  $a = 0.258$ ,  $T = 710\text{--}770^\circ\text{C}$ ,  $M = 6.6\%$ .

can then be approximated closely by

$$\Delta P = \rho_p g (1 - \bar{\epsilon}) \Delta h. \quad (4)$$

Hence, the suspension density can be estimated as

$$\rho_{\text{susp}} = \rho_p (1 - \bar{\epsilon}) = \Delta P / g \Delta h. \quad (5)$$

In the pilot tests, the suspension density was adjusted by draining solids from the system with the air ratio maintained constant. Suspension densities were measured below and above the secondary air injection level. The overall suspension density in the riser was taken as the weighted average of the two on a height basis.

Fig. 8 shows the effect of the overall suspension density on the gas heating value. The suspension density at the bottom of riser was between 100 and  $140 \text{ kg/m}^3$ . The gas heating value increased from  $3.5$  to  $4.7 \text{ MJ/Nm}^3$  as the overall suspension density increased from  $42$  to  $93 \text{ kg/m}^3$ . The solid line shows the best linear fit for all data points, with a correlation coefficient  $R^2 = 0.72$ . The positive influence of suspension density on gas quality is believed to be due to an increase in the concentration of solid reactants, together with enhanced solids mixing.

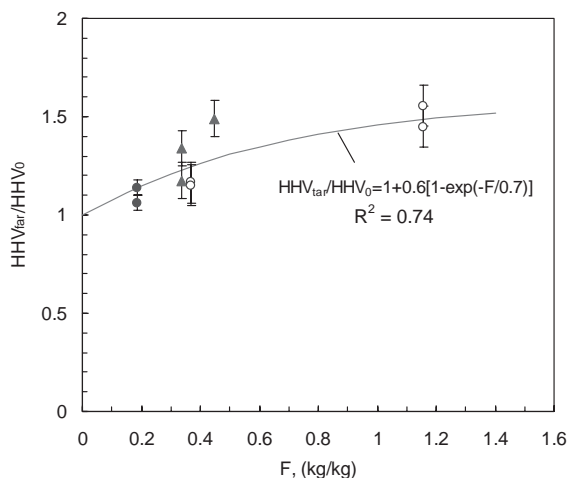


Fig. 9. Effect of fly ash re-injection on normalized gas heating value: ○—SPF/cypress mix,  $a=0.35$ ,  $T=700\text{--}740^\circ\text{C}$ ,  $M=11.3\%$ ; ▲—SPF/cypress sawdust,  $a=0.41$ ,  $T=720\text{--}760^\circ\text{C}$ ,  $M=15.0\%$ ; ●—Cedar/hemlock mix,  $a=0.40$ ,  $T=800\text{--}830^\circ\text{C}$ ,  $M=12.6\%$ .

### 2.7. Effect of fly ash re-injection

Since fly ash re-injection can increase suspension density as well as the carbon concentration in the riser, it should have a similar effect to raising the suspension density on gas quality and carbon conversion. To facilitate discussion, we first define

$$F = \frac{\dot{m}_{fa} C_{fa}}{\dot{m}_f C_f} \quad (6)$$

as the ratio of the carbon in re-injected fly ash to the carbon introduced with the fuel, where  $\dot{m}$  denotes dry feed rate and  $C$  is the fractional carbon content. Subscripts fa and f refer to fly ash and fuel, respectively. The carbon content in the ash retained in the riser was less than 2% for all runs, while it varied from 12% to 63% in the fly ash. This makes fly ash a major source of carbon loss if it is not recycled.

The gas heating value is plotted as a function of the carbon recirculation ratio,  $F$ , in Fig. 9. A simple, empirical correlation for the species and parameter range tested is

$$\text{HHV}_{\text{far}}/\text{HHV}_0 = 1 + 0.6[1 - \exp(-F/0.7)]. \quad (7)$$

Here the subscripts far and 0 stand for cases with and without fly ash re-injection, respectively. The correlation coefficient for this relationship is  $R^2 = 0.74$ . The effect of re-injection diminishes as  $F$  approaches zero.

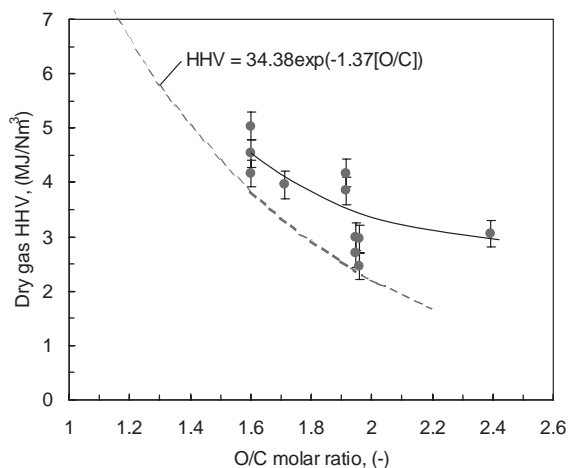


Fig. 10. Effect of steam injection rate on instantaneous dry gas heating values for hemlock sawdust.  $T=750\text{--}800^\circ\text{C}$ ,  $a=0.38\text{--}0.43$ ,  $M=8.8\text{--}9.2\%$ . Dashed line: best fit for no steam injection; solid line and data points: with steam injection.

The benefit of carbon re-injection reaches a limit due to kinetic limitations at a given temperature and solids residence time. It is expected that fly ash re-injection would be more beneficial at higher temperatures. Fly ash re-injection had little effect on the product  $\text{H}_2/\text{CO}$  and  $\text{CH}_4/\text{H}_2$  ratios. However, measured gas compositions indicate that for a given total oxygen/total carbon ratio, the  $\text{CO}/\text{CO}_2$  ratio increased with increasing re-injection.

### 2.8. Effect of steam injection and fuel-bound moisture

Fig. 10 shows that steam injection can significantly improve gas quality at a given O/C molar ratio. The steam injection rates tested were in the range 0–10.5 kg/h, resulting in an increase of 0–0.67 in the O/C molar ratio from the baseline cases with no steam injection. When steam is introduced,  $\text{CO}$  and  $\text{H}_2$  are formed as products of the endothermic steam-char reaction. As a result, steam injection makes the dry gas heating value higher than for purely air-blown processes at the same O/C ratio. This effect can also be seen from the product molar ratios, reflecting progress of the methane steam reforming and CO-shift reactions. However, in a gasification system without an external heat source, steam injection lowers the

operating temperature, and this could lead to a higher tar yield.

Steam, although injected at a higher level, caused greater changes in the product ratios, and showed much better reactivity, than an equal feed rate of fuel moisture. To produce hydrogen-rich gas from small units, it is desirable, where feasible, to employ steam injection. Alternatively, feeding sawdust in the recycle leg is likely to improve the ability of the moisture in the feed material to participate in the chemical reactions.

### 2.9. Effect of sawdust species and particle size

Notwithstanding differences in wood type, different sawdust species show greater uniformity in chemical composition (Table 1) than coal and other solid fossil fuels. For the six biomass species tested in the present study, species effects on gas heating value and carbon conversion were relatively minor from a chemical point of view. Nevertheless, the various sawdust species behaved differently during the gasification tests due to differences in physical properties, e.g. fibre length, moisture content, shape and particle size, caused by different methods of processing. For example, cedar hog fuel, because of its long fibre length, tended to cause bridging in the feed hoppers. Blending the ground cedar hog fuel with a more granular sawdust helped alleviate this tendency. The hemlock and cypress sawdusts proved to be most suitable for feeding because of their more favourable shape and low bridging tendency, even at relatively elevated moisture contents. Over the limited range tested in this work, particle size effects on gas heating value and carbon conversion were negligible.

### 2.10. Tar yield

The experimental data indicate that the tar concentration primarily depends on the operating temperature. Ultimate analysis of tar samples shows that typical tars contain about 78% carbon, 6% hydrogen, 0.7% nitrogen, 12% oxygen, less than 0.5% sulphur, and the rest being solids. The measured tar yield, shown in Fig. 11, decreased sharply from 15.2 g/Nm<sup>3</sup> at 700°C to 0.4 g/Nm<sup>3</sup> at 815°C. This arises because of increased tar cracking rates at higher temperatures. The results are approximately linear on semi-log pa-

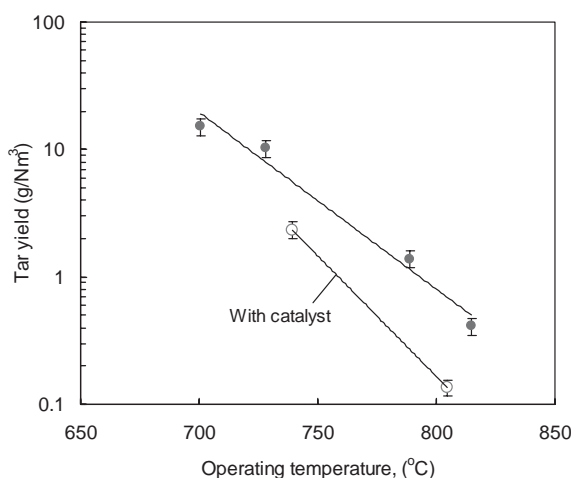


Fig. 11. Temperature dependence of tar yield and effect of nickel-based catalyst:  $a = 0.21\text{--}0.46$ ,  $T = 700\text{--}815^\circ\text{C}$ ,  $M = 4.18\text{--}14.7\%$ . ●—no catalyst; ○—with catalyst.

per suggesting an exponential decay function. Despite measures to reduce sampling losses, the uncertainty in tar measurement could be as large as 15% in practice. Fortunately, the experimental trends were not affected by such uncertainties. The results from this work are in qualitative agreement with those of previous studies [21,22]. Another set of data [18] although fitting our trend line well at higher temperatures, shows considerable scatter.

In addition to raising the operating temperature, it has been reported [22,23] that further tar reduction can be achieved by using commercial or mineral catalysts. In Run 14, 62% tar removal was achieved at a reactor temperature of 735°C by adding 11–14 kg nickel-on-alumina commercial steam-reforming catalyst. The tar yield was reduced to 0.15 mg/Nm<sup>3</sup> when the system operated at 800°C with catalyst addition. The catalyst activity increased as the operating temperature rose, with the result that the H<sub>2</sub> content increased with increasing temperature.

### 2.11. Mass and energy balances and gasification efficiency

Post-test mass and energy balances were performed to determine the carbon conversion and thermal efficiencies. A nitrogen balance was chosen as the primary basis for the mass balance because nitrogen is

the most abundant element in an air-blown gasification process, while it is relatively easy to determine accurately by experimental means, and it is largely independent of other elements. A secondary basis for the mass balance calculations is the oxygen balance, which helps diminish errors when the moisture content in the product gas is unknown or cannot be measured accurately. Alternatively, a hydrogen balance can be used as a secondary basis [18].

The carbon conversion is defined as the fraction of carbon in the feed converted to gaseous products. A modified carbon conversion can be defined which also accounts for the contribution of tars. The results of mass balances and gasification efficiency calculations appear in Table 2. For all fifteen runs in the pilot study, the overall mass balance gives 95–101% closure, with the corresponding ash balance giving 63–110% closure. Since the carbon balance is based on other elemental balances, it is difficult to achieve perfect closure.

The carbon conversion is determined from the product gas composition and gas yield. The air (or O/C) ratio was the primary factor influencing carbon conversion. A simple correlation for the experimental carbon conversion vs. air ratio is

$$C = 0.25 + 0.75[1 - \exp(-a/0.23)] \quad (8)$$

(0.22 ≤ a ≤ 0.54).

The correlation coefficient ( $R^2$ ) of Eq. (8) is 0.86. Temperature and residence time are not included in this equation because of their relatively weak influences and the limited number of data points. Comparison of our test results with those of a previous study [16] shows substantial agreement in the trend, despite a difference of ~ 5% in the absolute carbon conversion. The latter difference likely arises from differences in reactor configuration, cyclone efficiency, fuel moisture content in the fuel and operating temperature.

A cold-gas efficiency is used to evaluate the gasification performance. The cold-gas efficiency,  $E_1$ , excluding the heating value of the condensables (tars), is defined as the percentage of the fuel heating value converted into the heating value of the product gas, i.e.

$$E_1 = \frac{[\text{HHV}]_g \times v_g}{[\text{GCV}]_f} \times 100\%, \quad (9)$$

where  $[\text{HHV}]_g$  (in MJ/Nm<sup>3</sup>) is the higher heating value of the product gas, while  $[\text{GCV}]_f$  (in MJ/kg) denotes the gross calorific values of the fuel;  $v_g$  is the specific dry gas volume, in Nm<sup>3</sup>/kg fuel.

A modified cold-gas efficiency, now including the heating value of any tars, is

$$E_2 = \frac{[\text{HHV}]_g \times v_g + [\text{HHV}]_t \times y_t}{[\text{GCV}]_f} \times 100\%. \quad (10)$$

Here  $y_t$  is the specific tar yield in kg/kg-fuel, and  $[\text{HHV}]_t$  is the heating value of tar, taken as 30.1 MJ/kg-tar, estimated from the tar analysis data.  $E_1$  and  $E_2$  have both been used extensively in the gasification literature [e.g. [24,25]].

Calculated gasification efficiencies are given in the last two rows of Table 2. In the present study, since the enthalpy of the product gas and hot water produced by the heat exchangers is not utilized in any downstream equipment, nor is the reactor externally heated, the cold-gas efficiency is adequate to assess the performance of the process. However, external heat may be required to maintain the operating temperature. The cold gas efficiency, which does not account for the external heat supply, then becomes insufficient to measure gasifier performance.

The gasification efficiencies  $E_1$  and  $E_2$  calculated from the mass and energy balance are plotted in Fig. 12

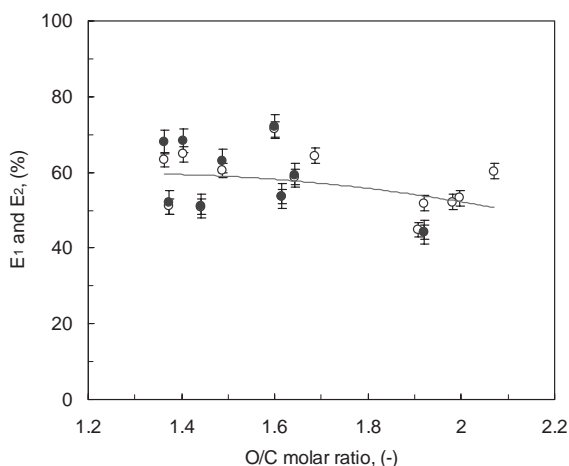


Fig. 12. Variation of gasification efficiency with O/C ratio.  $a=0.21$ – $0.54$ ,  $T=700$ – $815^\circ\text{C}$ ,  $M=4.2$ – $22.0\%$ . ○— $E_1$ , only product gas considered; ●— $E_2$ , tar also taken into account.

Table 2  
Summary of mass balance and gasification efficiency calculations

Run number		1	2	3	4	5	6	7	8	9	10	11	12	13	14	15
Sawdust species		cyp.	cyp.	SPF	hem.	hem.	hem.	hem.	SPF/C	hem.	c/h	hem.	PS	mixed	mixed	mixed
Total gasification run time h		3.80	4.53	3.00	4.23	4.10	4.27	2.62	3.57	3.62	3.58	3.80	2.42	3.07	3.98	3.55
Sawdust consumption	kg	91.0	103.8	80.7	110.6	118.6	108.2	88.1	126.3	112.3	95.4	120.8	117.3	140.0	164.8	55.2
Moisture content in sawdust	%	22.0	9.7	10.5	10.0	8.8	9.2	11.7	11.3	15.0	12.6	14.7	10.1	6.6	6.7	4.2
Throughput, dry basis	kg/s m <sup>2</sup>	0.87	0.97	1.13	1.10	1.23	1.08	1.39	1.47	1.23	1.09	1.27	2.04	1.99	1.81	0.70
Total air supplied	Nm <sup>3</sup>	310	255	177	281	226	225	142	207	207	179	186	125	188	251	135
Fly ash re-injection	kg	0	0	0	0	0	0	0	16.8	20.0	5.2	0	0	0	0	0
Total steam injection	kg	0	0	0	0	2.86	24.17	0	0	0	0	0	0	0	0	0
Mean suspension temp. (T <sub>3</sub> )	C	740	718	766	815	772	787	718	730	752	815	789	701	728	739	805
Primary air pressure	bar	1.65	1.19	1.19	1.19	1.19	1.19	1.19	1.19	1.19	1.19	1.19	1.19	1.19	1.19	1.19
Time-mean air ratio	–	0.536	0.445	0.402	0.522	0.376	0.427	0.340	0.350	0.411	0.399	0.337	0.218	0.258	0.294	0.460
<i>Mean gas composition (dry basis)</i>																
H <sub>2</sub>	%	5.6	3.1	3.2	3.0	4.0	3.8	5.5	3.9	3.5	4.1	4.2	5.4	5.1	7.3	5.9
N <sub>2</sub>	%	68.0	68.1	67.1	68.4	61.8	65.2	59.5	62.5	64.8	64.6	62.6	53.9	56.3	55.4	64.6
CO	%	6.9	11.0	10.7	9.6	14.7	12.6	16.6	15.1	13.4	12.3	14.6	21.4	19.9	17.9	10.0
CH <sub>4</sub>	%	1.4	1.9	1.9	1.9	2.9	2.7	3.4	2.8	2.8	2.5	3.0	4.6	4.1	3.2	1.2
CO <sub>2</sub>	%	18.1	15.9	17.1	17.1	16.5	15.7	15.0	15.6	15.6	16.5	15.7	14.7	14.5	16.3	18.3
<i>Mean dry gas heating value</i>																
value	MJ/Nm <sup>3</sup>	2.43	2.96	2.92	2.75	4.14	3.73	4.82	4.13	3.85	3.59	4.17	6.13	5.62	4.60	2.54
Gas yield	Nm <sup>3</sup> /kg	3.30	2.92	2.48	3.10	2.59	2.75	2.34	2.27	2.46	2.51	2.13	1.72	2.06	2.35	3.24
Tar yield	g/Nm <sup>3</sup>	n. a.	0.41	1.39	15.13	10.26	2.35	0.04								
<i>Overall mass balance</i>																
closure	%	98.3	99.6	97.7	98.4	97.8	98.7	98.0	96.9	98.7	97.5	98.7	100.5	100.7	100.1	95.4
Carbon conversion, gas	%	97.7	102.0	92.9	99.2	98.6	93.0	91.9	85.8	91.1	87.6	81.9	81.6	89.8	94.9	98.3
Carbon conversion, gas + tar	%	n. a.	87.7	82.4	85.7	93.1	95.8	98.3								
Cold-gas efficiency, E <sub>1</sub>	%	53.2	51.8	44.8	52.2	64.3	60.3	71.4	51.0	50.8	53.6	58.7	63.3	64.7	60.5	44.2
<i>Overall thermal efficiency, E<sub>2</sub></i>																
E <sub>2</sub>	%	n. a.	53.8	59.3	67.9	68.2	61.5	44.2								

Notes: cyp. = cypress; SPF = spruce-pine-fir mixture; hem. = hemlock; SPF/C = SPF/cypress mixture; c/h = mixed cedar-hemlock; PS = mixed pine bark-spruce.

against the O/C molar ratio. Results suggest that O/C should be in the range 1.3–1.6 to maximize gasification efficiency for the species and parameters tested. Compared to carbon conversion, the gasification efficiencies give a better measure of the performance of the gasifier.

### 3. Equilibrium modelling

At chemical equilibrium a reacting system is at its most stable composition, a condition achieved when the entropy of the system is maximized, while its Gibbs free energy is minimized. Two approaches have been developed for equilibrium modelling: stoichiometric and non-stoichiometric [26]. The stoichiometric approach requires a clearly defined reaction mechanism incorporating all chemical reactions and species involved. In a non-stoichiometric formulation, on the other hand, no particular reaction mechanism or species are involved in the numerical solution. The only input needed to specify the feed is its elemental composition, which can be readily obtained from ultimate analysis data. This method is particularly suitable for problems with unclear reaction mechanisms and feed streams like biomass whose precise chemical compositions are unknown.

The pilot-scale gasifier described above operated under near-steady-state conditions and was subject to axial and radial gradients of temperature and composition. In the equilibrium model, however, the reactor is implicitly considered to be zero-dimensional, i.e. no spatial distribution of parameters is considered, nor are there changes with time because all forward and reverse reactions have reached chemical equilibrium. The molar inflow for any individual element involved in the chemical reactions can then be written as the sum of moles of that element in the various feed streams. Tars are not included in the product stream because of their low yield for the conditions considered.

To simplify the problem, only 42 gaseous and 2 solid species involving C, H, O, N and S are considered in the present work. Other elements (e.g. Si entering as SiO<sub>2</sub>, and mineral matter in the biomass) are considered to be inert or independent of the reaction system. Although carbon, oxygen and sulphur may be present in mineral matter (e.g. as carbonates

and sulphates), and may be converted during gasification, inorganic C, O and S are minor contributors to the elemental abundance of the system because of the low ash content of the biomass concerned. Little error therefore results when they are ignored in equilibrium modelling.

Although our major concern in the present work is the phenomenological model, which is adapted from the pure equilibrium model, both models share the same mathematical basis. The pure equilibrium model is first introduced. Followed by the justification and methodology of incorporating non-equilibrium factors.

#### 3.1. Formulation of pure equilibrium model

The RAND algorithm which has been well-documented in previous literature [26–28] is used in the present work. Validation of the method was described in our previous work [29], in which it was used successfully to predict the performance of a coal gasifier. In the RAND algorithm, the change in moles of a species in the  $m$ th iteration can be expressed explicitly as a function of its current chemical potential, the phase distribution of the species at a given system temperature and pressure, and the Lagrange multiplier:

$$\begin{aligned} \delta n_i^{(m)} &= n_i^{(m)} \left( \sum_{k=1}^K a_{ik} \psi_k + u_\alpha - \frac{\mu_i^{(m)}}{RT} \right) \\ &\text{for multi-species phases,} \\ &= u_\alpha n_i^{(m)} \quad \text{for single-species phases} \\ &(i = 1, 2, \dots, N, \quad k = 1, 2, \dots, K, \\ &\quad \alpha = 1, 2, \dots, \pi). \end{aligned} \quad (11)$$

These  $\delta n_i^{(m)}$  constitute a vector  $\delta \mathbf{n}^{(m)}$ , which is the change of number of moles for all species upon the current iteration.  $N$  designates the total number of species.  $\mu_i^{(m)}$  and  $n_i^{(m)}$  denote the chemical potential and moles of species  $i$  in the  $m$ th iteration, respectively.  $a_{ik}$  is the coefficient in the species-element matrix;  $\psi_k$  is a function related to the Lagrange multiplier,  $\lambda_k$ , i.e.

$$\psi_k = \frac{\lambda_k}{RT} \quad (12)$$

$u_\alpha$  is the phase split of  $\delta n_i$ , defined as

$$u_\alpha = \sum_{i=1}^N \delta n_{i\alpha}^{(m)} / n_i^{(m)} = \delta n_{t\alpha}^{(m)} / n_t^{(m)}, \quad (13)$$

where subscript  $t$  means total and  $\alpha$  refers to the phase to which a species belongs.

The set of  $(K + \pi)$  simultaneous algebraic equations that are to be solved iteratively by the RAND algorithm includes  $K$  linear equations regarding element abundance:

$$\begin{aligned} \sum_{k=1}^K \sum_{i=1}^N a_{ik} a_{ij} n_i^{(m)} \psi_k + \sum_{\alpha=1}^{\pi} b_{j\alpha}^{(m)} u_\alpha \\ = \sum_{i=1}^N a_{ij} n_i^{(m)} \frac{\mu_i^{(m)}}{RT} + b_k - b_k^{(m)} \\ (j = 1, 2, \dots, K). \end{aligned} \quad (14)$$

The  $\pi$  supplementary equations for different phases are:

$$\begin{aligned} \sum_{k=1}^K b_{k\alpha}^{(m)} \psi_k - n_{z\alpha} u_\alpha = \sum_{i=1}^N n_{i\alpha}^{(m)} \frac{\mu_{i\alpha}^{(m)}}{RT} \\ (\alpha = 1, 2, \dots, \pi). \end{aligned} \quad (15)$$

The initial element abundance vector  $b$  is calculated from the feedstock. The  $k$ th element of the  $b$ -vector at the  $m$ th iteration is

$$b_k^{(m)} = \sum_{i=1}^N a_{ik} n_i^{(m)}. \quad (16)$$

Mass balance constraints are imposed at every iteration during solution of Eqs. (11)–(16), while the algorithm iteratively minimizes the Gibbs free energy. The difference between the initial elemental abundance vector and its current iteration value ( $b_k - b_k^{(m)}$ ), is added to the right-hand side of Eq. (14) to eliminate error accumulation during the iteration process [26].

Finally, the new numbers of moles vector,  $\mathbf{n}^{(m+1)}$ , is determined by

$$\mathbf{n}^{(m+1)} = \mathbf{n}^{(m)} + \omega^{(m)} \delta \mathbf{n}^{(m)}, \quad (17)$$

where  $\omega^{(m)}$  is the step size parameter,  $0 < \omega^{(m)} < 1$ , chosen such that all new moles generated from the current iteration remain positive. The new molar fractions of all species are then determined by

$$x_i = n_i / n_t. \quad (18)$$

Other quantities, such as elemental distributions, carbon conversion and water conversion, are all derived from the variables in Eq. (18). The convergence criterion is that the maximum absolute value of the changes in the molar fractions for all species is less than a pre-set upper limit, typically  $1 \times 10^{-6}$  molar, to ensure good accuracy as well as a true global minimum of the Gibbs free energy.

The energy balance of the process can be written

$$\begin{aligned} \sum_{l=1}^L \dot{m}_l \Delta H_{f,298,\text{feed}}^0 + \sum_{l=1}^L \dot{m}_l H_{\text{feed}}(T_{\text{feed},l}) \\ = \sum_{i=1}^N n_i \Delta H_{f,298,\text{prod}}^0 + \sum_{i=1}^N n_i H_{\text{prod}}(T) \\ + \Delta H(T) \quad (l = 1, 2, \dots, L) \end{aligned} \quad (19)$$

for any temperature  $T$ . The two terms on the left-hand side are the total heat of formation and the total enthalpy of all feed streams, respectively. The first two terms on the right-hand side represent the total heat of formation and total enthalpy of all product species, respectively. The final term denotes the system net energy excess production as a function of temperature. This term can also be extended to account for any heat removed from the reactor or provided by an external heat source. If  $\Delta H(T)$  is positive, the system adjusts its equilibrium temperature to a higher level. The equilibrium temperature of the system is the temperature at which  $\Delta H(T) = 0$ . Eq. (19) is based on 1 kg of fuel (dry basis). Note that although  $m_l$  and  $n_i$  have different units, all the terms on both sides of the equation are converted into MJ by multiplying by enthalpies expressed in MJ/Nm<sup>3</sup>, MJ/kg or kJ/mol as needed.

The ultimate analysis of a typical sawdust used in the model calculations, listed in the last column of Table 1, is obtained by averaging the analyses of six sawdust species. The heats of formation of the oxidant and steam can be determined from standard thermodynamic data [30]. The heat of formation of fuel, in kJ/kg fuel as received, is calculated from the equation [29]

$$\begin{aligned} \Delta H_{f,298,\text{fuel}}^0 = \text{HHV} - (327.63 C_{\text{ar}} + 1417.94 H_{\text{ar}} \\ + 92.57 S_{\text{ar}} + 158.67 M_{\text{ar}}), \end{aligned} \quad (20)$$

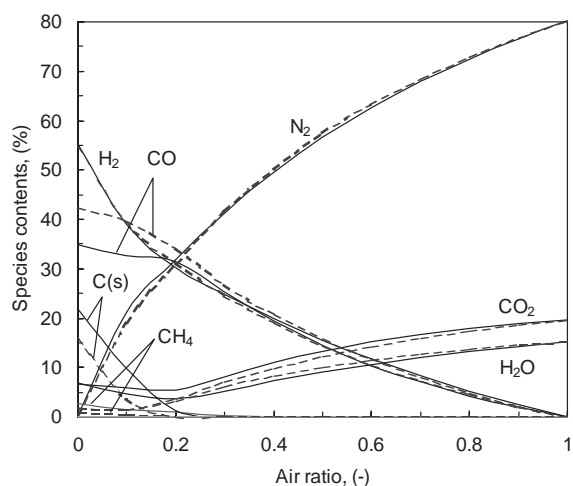


Fig. 13. Variation of equilibrium gas composition with air ratio for representative sawdust composition at a pressure of 1.013 bar. Solid lines—1000 K, dashed lines—1100 K. No steam added.

where HHV denotes the higher heating value of the fuel (kJ/kg, as-received basis).  $C_{ar}$ ,  $H_{ar}$ ,  $S_{ar}$  and  $M_{ar}$  represent the carbon, hydrogen, sulphur and moisture contents of the fuel (wt%, as-received basis), respectively. This equation assumes that  $CO_2$ ,  $H_2O$  and  $SO_2$  are the only combustion products.

### 3.2. Predicted species concentrations

Fig. 13 shows predictions of the dependence of the molar contents of 7 major species on air ratio when the representative sawdust is gasified at 1.013 bar. Five species ( $H_2$ ,  $N_2$ ,  $CO$ ,  $CO_2$  and  $CH_4$ ) are given by their molar fractions in the dry product gas.  $H_2O(g)$  is shown by its concentration in the wet gas, while unconverted carbon,  $C(s)$ , is represented by its molar fraction in the overall equilibrium system. The numerical predictions in the present work covered the temperature range 600–1600 K. However, to minimize clutter, predictions are presented here only for 1000 and 1100 K.

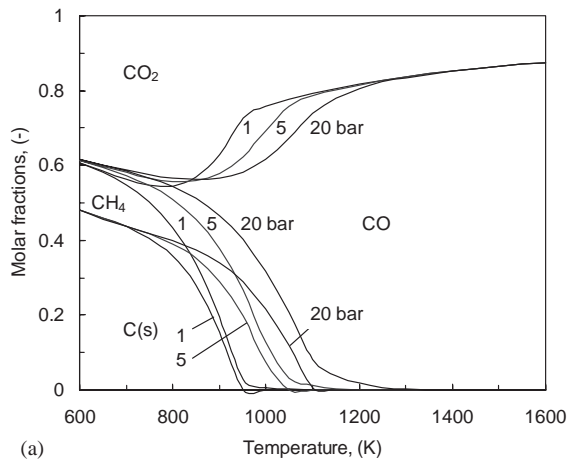
As expected, major oxidizing species ( $CO_2$ ,  $H_2O$ ) increase with increasing air ratio, while reducing species ( $H_2$ ,  $CH_4$ ,  $CO$ ) decrease. The model predicts that the equilibrium content of methane should not exceed 3% at temperatures above 1000 K, even with no air supplied. For typical gasification conditions ( $a = 0.3$ ), the equilibrium  $CH_4$  concentration

is only 0.02% for a temperature of 1100 K. Measured methane contents significantly higher than this level arise from incomplete cracking of the pyrolysis products. The  $CO_2$  and  $H_2O$  concentrations decrease slightly with increasing air ratio below 1000 K for  $a < 0.2$ . This is due to the rapid disappearance of unconverted carbon  $C(s)$  with increasing air ratio, which causes rapid growth in the total moles in the gas phase. At 1100 K, the initial fraction of unconverted carbon is smaller than at 1000 K, and the decreasing trend for  $CO$  and  $H_2O$  vs. air ratio at low air ratios nearly disappears.

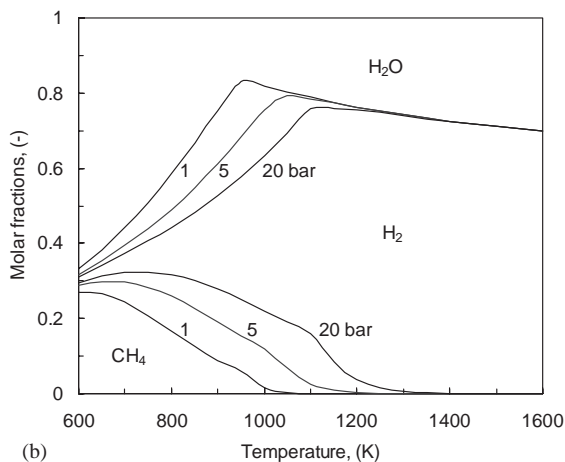
### 3.3. Elemental distribution in products

The fate of elements in the feedstock can be interpreted in terms of the distribution of fractions converted to different species in the spectrum of final products, as shown in Fig. 14. These fractions must add up to unity. Fig. 14(a) plots the predicted carbon distribution versus operating temperature for  $a = 0.3$  at different pressures. The height under the lowest curve for each pressure represents the molar fraction of unconverted solid carbon,  $C(s)$ . The narrow band between this curve and the next higher one for the same pressure gives the mole fraction of hydrocarbons, mostly  $CH_4$ . The interval to the next curve for the same pressure signifies  $CO$ , while the region above the highest corresponding curve is occupied by  $CO_2$ . The equilibrium model indicates that pressure should only affect the carbon distribution for intermediate temperatures from  $\sim 700$  to 1250 K. Beyond this range, the system pressure again becomes a secondary factor. At 1000 and 1100 K, atmospheric pressure, and air ratios below 0.2, a considerable portion of the carbon may remain as solid carbon. For  $0.2 < a < 0.3$ , there is little change in the  $CO$  content due to the gradual disappearance of solid carbon, suggesting that this is a desired range of operation for producing  $CO$ -rich gas.

The hydrogen distribution is shown in Fig. 14(b).  $CH_4$  occupies a significant part of the equilibrium product spectrum at low air ratios and temperatures less than about 1000 K. The predictions show that an equilibrium-controlled atmospheric biomass gasification process intended to produce hydrogen-rich gas should operate in the temperature range from 1100 to 1300 K and at an air ratio from 0.15 to 0.25 to



(a)



(b)

Fig. 14. Predicted effects of temperature and pressure on elemental distributions: (a) carbon distribution for  $a = 0.3$ ; (b) hydrogen distribution for  $a = 0.3$ .

maximize hydrogen production. For larger air ratios,  $\text{H}_2\text{O}$  starts to dominate the hydrogen distribution as a net product of hydrogen oxidation.

The oxygen distribution in the system indicates that more than half of the oxygen supply is used to produce  $\text{CO}_2$  and water for an air ratio larger than 0.33. Operation below this air ratio is therefore preferable. In addition to fuel drying, good insulation, air preheating and natural gas augmentation may help maintain an elevated system temperature.

The limited pressure influence on the product distributions of the three most abundant elements (C, H, and O) implies that high-temperature gasification

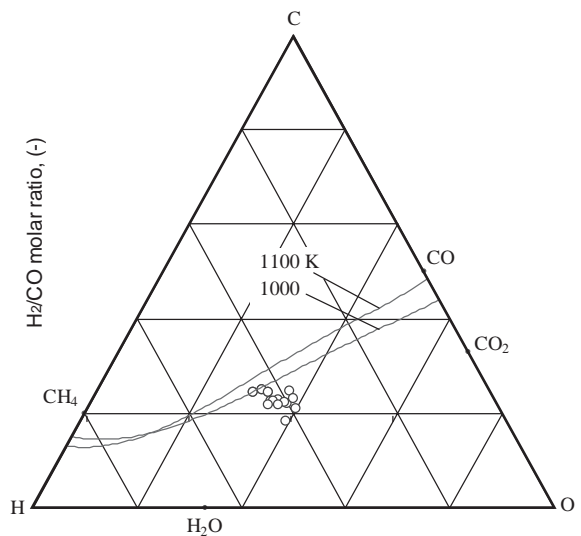


Fig. 15. Carbon formation tendency in sawdust gasification: data from CFB pilot tests (Runs 1–15) gasifying six sawdust species.

( $T > 1200 \text{ K}$ ) does not require elevated pressures since increasing pressure only increases the energy consumption with little gain in equilibrium product quality. The same holds for very low-temperature processes ( $T < 700 \text{ K}$ ) such as those using supercritical water as oxidizing agent, or anaerobic processes. However, high pressure does concentrate the gas phase and accelerate reactions while reducing reactor volume and the time required to achieve equilibrium.

### 3.4. Carbon formation tendency in biomass gasification

Previous work [29] by the authors discussed the nature of carbon formation in coal gasification systems and predicted carbon formation boundaries for different operating temperatures and pressures. As in that work, a biomass gasifier can be represented by a C–H–O ternary system since nitrogen is almost inert, and the molar abundance of sulphur is two or three orders of magnitude smaller than those of the other four major elements. In Fig. 15, the elemental abundance combinations from our experimental study are represented by open points. Only three points fall in the boundary zone, with none residing in the carbon-forming regime. Therefore, the presence of

unconverted solid carbon must be attributed solely to kinetic, mass transfer and gas–solid separation limitations.

For a given elemental abundance combination, when more air is supplied, the system moves along a straight line toward the pure oxygen (O) vertex. When the moisture content of the fuel increases or when steam is injected, the system migrates towards the H<sub>2</sub>O point. When fly ash is re-injected, the abundance of carbon increases without causing much change in the abundance of H and O since fly ash consists mostly of carbon. Hence, the system travels toward the C vertex, leading to an increased tendency to form carbon.

### 3.5. Deviations from chemical equilibrium

Previous work [31] has reported deviations in gas composition from equilibrium predictions for several types of gasifiers. The best-fit equilibrium temperature,  $T_{\text{eq}}^0$  based on an equilibrium model, tends to deviate from the reported operating temperature. The best-fit temperature is defined here as the temperature which minimizes the sum of squares of the deviations for five principal gas species (H<sub>2</sub>, CO, CO<sub>2</sub>, CH<sub>4</sub>, N<sub>2</sub>), i.e.

$$T_{\text{eq}}^0 = T \quad \text{at} \quad \min \left| \sum (y_{\text{eq}} - y_{\text{meas}})^2 \right|. \quad (21)$$

The larger the temperature deviation, the farther the system is from chemical equilibrium. At full chemical equilibrium, the deviation between the actual temperature and  $T_{\text{eq}}^0$  should disappear. Therefore, the difference between the best-fit  $T_{\text{eq}}^0$  value and the representative actual temperature (e.g. cyclone exit temperature) can be used as a measure of the approach to equilibrium.

Comparing the carbon conversion data from our pilot tests with equilibrium predictions, one can find a similar shift towards the low-temperature side. The deviation from equilibrium conditions indicates that a higher operating temperature is required to reach a given solid conversion than is thermodynamically necessary.

Previous studies [32,33] have shown that high measured concentrations of methane from coal gasification result from incomplete conversion of pyrolysis products; equilibrium molar concentrations of methane in the off-gas are less than 0.1% for the entire parameter

range tested, whereas actual methane concentrations are of the order of a few per cent. The high measured methane concentration in the product gas cannot be explained on an equilibrium or thermodynamic basis. Once again, the deviation must result from one or more non-equilibrium factor, e.g. incomplete cracking of pyrolysis products.

## 4. Modified model and comparison with experimental results

### 4.1. Elemental availability and modified model

The element abundance vector of the feed can be written

$$b_0 = (n_C, n_H, n_O, n_N, n_S). \quad (22)$$

It is often taken for granted that the amount of each element participating in the chemical equilibrium is exactly the same as in the feed. This is true when the reaction kinetics and mass transfer processes do not impede the achievement of equilibrium. However, this assumption is not valid for real processes in which reactions (mostly heterogeneous) are influenced by kinetics and/or mass transfer so that some elements never achieve equilibrium.

The previous section showed deviations of our real gasifier from chemical equilibrium. This suggests that an equilibrium-based model that does not consider such deviations is liable to substantial error in predicting gas composition and overall efficiency. However, equilibrium models are useful as design tools, able to explore process behaviour under thermodynamic control. In order to correct for the deviations in real gasification systems, a phenomenological model was developed in this work by modifying an equilibrium-based framework to account for key non-equilibrium factors.

If the experimental carbon conversion and methane yield are available, one can correct for non-equilibrium effects by withdrawing the corresponding carbon and hydrogen from the equilibrium system. This method was applied successfully to coal gasification [29], and it was also successful for steam methane reforming [34] where hydrogen was preferentially removed through perm-selective membranes. A phenomenological model is then established which

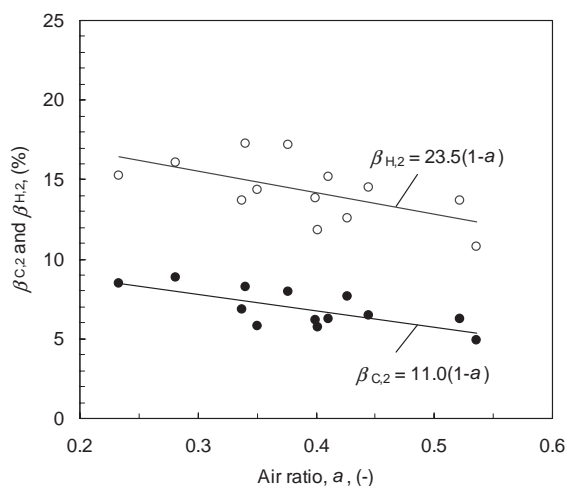


Fig. 16. Effect of air ratio on the percentages of carbon and hydrogen that remain as methane in the product gas. Data from Runs 1–15.  $a = 0.21\text{--}0.54$ ,  $T = 700\text{--}815^\circ\text{C}$ ,  $M = 4.2\text{--}22.0\%$ .

employs empirical data from the pilot-plant study to account for factors which prevent equilibrium from being achieved. In the present study, this approach is extended to account for non-equilibrium effects of pyrolysis products such as methane and carbon, and the modified equilibrium model is then applied to biomass gasification.

An availability function,  $\beta$ , is imposed on each element, leading to a modified element abundance vector affecting the gas, i.e.:

$$b^* = (\beta_{Cn_C}, \beta_{Hn_H}, \beta_{On_O}, \beta_{Nn_N}, \beta_{Sn_S}). \quad (23)$$

Based on experimental results from our pilot plant tests (Table 2), the fraction of carbon converted into gaseous species is

$$\beta_{C,1} = 0.25 + 0.75 \exp(-a/0.23). \quad (24)$$

However, a fraction of the carbon entering the gas phase exists as methane, produced during the pyrolysis stage and leaving the system without achieving equilibrium. Mass balance calculations for the pilot tests in this work (Fig. 16) suggest that this fraction can be approximated by

$$\beta_{C,2} = 0.11(1 - a). \quad (25)$$

Both  $\beta_{C,1}$  and  $\beta_{C,2}$  are based on the molar abundance of carbon in the feed. The portion of carbon consumed to produce methane must be deducted from the overall

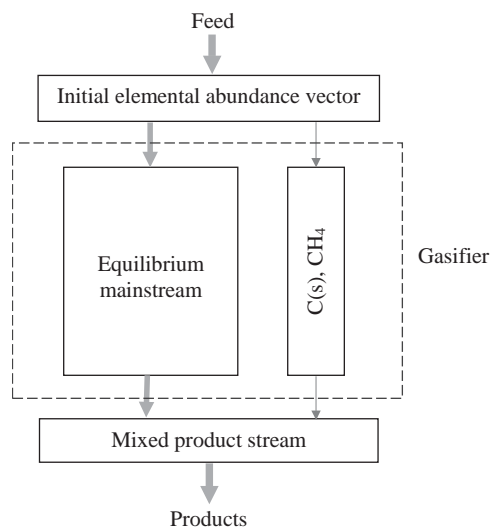


Fig. 17. Schematic of kinetic modification of equilibrium model.

fraction of carbon in the gas phase. The availability of carbon, i.e. the overall fraction of carbon entering chemical equilibrium, is therefore

$$\beta_C = \beta_{C,1} - \beta_{C,2}. \quad (26)$$

Since one mole of methane contains four moles of hydrogen atoms, the corresponding availability of hydrogen at equilibrium is

$$\beta_H = 1 - \frac{4\beta_{C,2}n_C}{n_H}. \quad (27)$$

The remaining error in the predictions can be attributed to failure to achieve complete conversion for other elements, as well as measurement errors. Since there is no systematic method for handling incomplete conversion of elements other than carbon, as a first approximation, we assume complete conversion for all elements other than carbon and hydrogen. Thus, Eq. (23) is reduced to

$$b^* = (\beta_{Cn_C}, \beta_{Hn_H}, n_O, n_N, n_S). \quad (28)$$

The modified equilibrium model is illustrated schematically in Fig. 17. The reaction system is assumed to be comprised of a mainstream in chemical equilibrium and a bypass zone, controlled by non-equilibrium factors. The effective abundances of carbon and hydrogen in the equilibrium main stream are clearly less than those computed from the feed. Consequently, the effective air ratio exceeds that

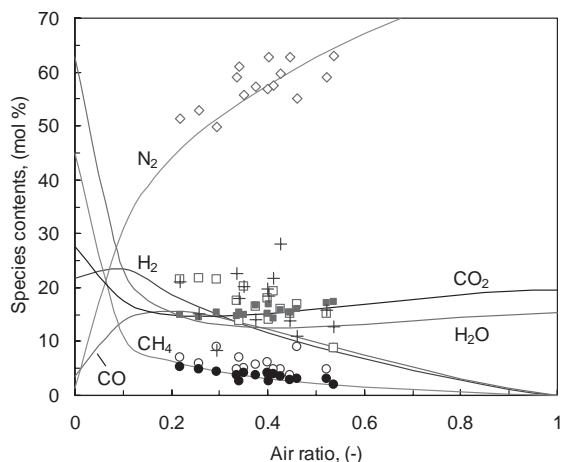


Fig. 18. Comparison between species molar contents predicted by the modified equilibrium model and measured data for a temperature of 1100 K. Legends:  $\circ$ — $H_2$ ,  $\bullet$ — $CH_4$ ,  $\square$ — $CO$ ,  $\blacksquare$ — $CO_2$ ,  $+$ — $H_2O$ ,  $\diamond$ — $N_2$ . For experimental details see Table 2.

based on the overall stoichiometry. The modified  $b^*$  gives a much-improved approximation of the actual element abundance entering equilibrium, leading to substantially better predictions.

#### 4.2. Comparison with experimental results

Fig. 18 shows the variation of gaseous species contents with air ratio predicted by the modified model, compared with the measured data. While  $N_2$  is predicted to be similar to that from the pure equilibrium model, significant changes are found in  $H_2$ ,  $CH_4$ ,  $CO$ ,  $CO_2$  and  $H_2O$ . As in Fig. 13, all species are dry-gas molar contents except for  $H_2O$ . The modified model predicts much higher  $CH_4$  and  $H_2O$  contents than the pure equilibrium model. In addition, the predicted concentrations of  $H_2$  and  $CO$  now go through maxima, not seen in the pure equilibrium predictions.

Very little difference is found between predictions for 1000 and 1100 K, so only the latter are plotted. Predictions for the  $CH_4$  content agree very well with experimental data. The predicted  $H_2$  molar content remains higher than the experimental data except for a few cases. Similar deviations for  $H_2$  were observed in previous work [13]. The main reason for this deviation is likely to be the fractional availability of water to the water–gas shift reaction. This reaction is moderately

exothermic ( $\Delta H_{298}^0 = -41.1$  kJ/mol  $CO$ ), so that its equilibrium constant decreases with increasing temperature. Therefore, the  $H_2/CO$  molar ratio may fall below 1 at high temperatures. The hydrogen produced by the shift reaction is over-predicted if all the water in the system is assumed to reach chemical equilibrium.

$CO$  contents are under-predicted by the modified model with a relative difference of 20–25%, while predicted  $CO_2$  contents are in good agreement with experimental data. Since  $H_2$  contents are over-predicted, while  $CO$  contents are under-predicted, the resulting  $H_2/CO$  molar ratios are significantly higher than the measured data, except for one test run with a particularly high moisture content in the fuel (22.0%). Good agreement is found between measured and predicted  $N_2$  and  $H_2O$  contents in the product gas.

Part of the deviation also comes from the assumption that all the unconverted carbon stays as  $C(s)$  or pure graphitic carbon. However, in real processes, the unconverted carbon usually occurs as coke ( $CH_x$ ,  $0 < x < 1$ ), which decreases the availability of both carbon and hydrogen. Further improvements in this respect should be sought in future work. However, it is encouraging that the modified equilibrium model gives much better predictions than the pure equilibrium model.

Fig. 19 compares the predicted gas heating value with the measured data. The dashed lines are calculated from the pure equilibrium model, while the solid line shows predictions of the modified model. An exponential correlation of gas heating value with air ratio (as shown in Fig. 6) seems quite reasonable for fitting experimental data over the range  $0.2 \leq a \leq 0.5$ . There is good agreement between the measured data and those predicted by the modified equilibrium model. The error in the predicted  $H_2/CO$  molar ratio in the product gas has little influence on the resulting gas heating value, owing to the fortuitous similarity of the heats of combustion of  $H_2$  and  $CO$  (286 and 283 kJ/mol, respectively).

The measured and predicted cold gas efficiencies are compared in Fig. 20. Again, the dashed lines are calculated from the pure equilibrium model, while the solid line shows the prediction of the modified model. A striking feature is the existence of a maximum cold gas efficiency at a non-zero air ratio for both versions of the model. The operating temperatures in the experimental study varied from  $\sim 1000$  to

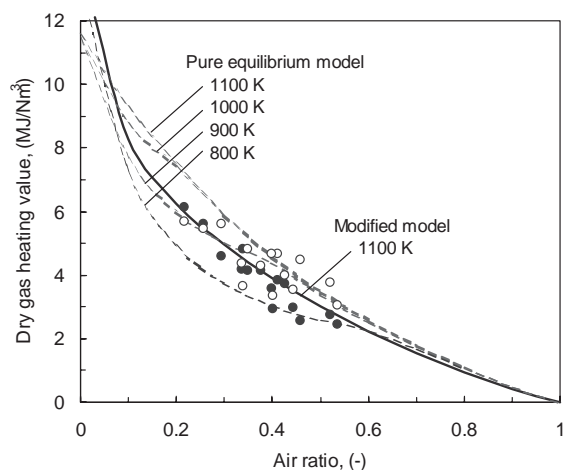


Fig. 19. Effect of air ratio on predicted and experimental dry gas heating value from sawdust gasification at 1.013 bar. Dashed lines: pure equilibrium model predictions; solid line: modified model prediction for 1100 K. Experimental data:  $a = 0.22$ – $0.54$ ,  $M = 4.2$ – $22.0\%$ ,  $T = 970$ – $1090$  K.  $\circ$ —best cases;  $\bullet$ —time-mean values.

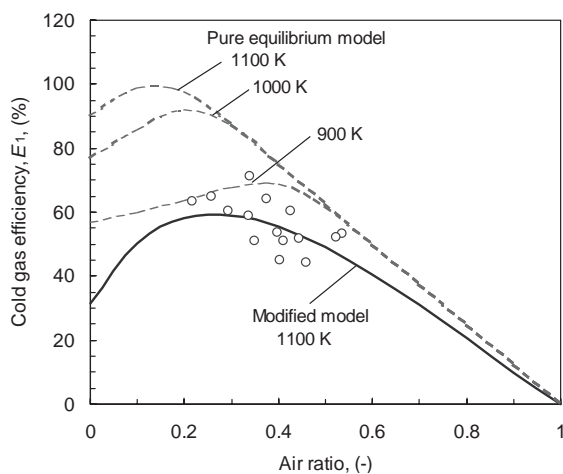


Fig. 20. Effect of air ratio on predicted and experimental cold-gas efficiencies from sawdust gasification at 1.013 bar. Dashed lines: pure equilibrium model predictions for 1100 K.  $a = 0.22$ – $0.54$ ,  $M = 4.2$ – $22.0\%$ ,  $T = 970$ – $1090$  K.  $\circ$ —time-mean values.

1100 K. Therefore, maximum gasification efficiency could only be expected for  $a < 0.3$ , though the pure equilibrium model predicts lower optimum air ratios for different operating temperatures. The modified

model is much more successful. Despite scatter, the experimental data are in substantial agreement with the modified model predictions.

## 5. Conclusions

- (1) Pilot plant tests of biomass gasification indicate that the product gas composition and heating value depend heavily on the air or O/C ratio and suspension temperature. Gas heating value can be increased by increasing the suspension density. Ash re-injection improved carbon conversion, while steam injection improved the quality (i.e. heating value) of the product gas.
- (2) While carbon conversion increased with increasing O/C molar ratio, the cold-gas gasification efficiency decreased. Gasification efficiency was maximized within an optimum range of air ratio (O/C = 1.3–1.6, or  $a = 0.25$ – $0.33$ ), while keeping the tar yield relatively low. Tar yield decreased exponentially with increasing operating temperature. Addition of a reforming catalyst significantly reduced tar yield, while secondary air had only a very limited effect on tar removal for a constant total air ratio.
- (3) The non-stoichiometric equilibrium model developed in this study predicts that the product gas composition depends primarily on the air ratio. Pressure only influences the results significantly over a limited temperature range (750–1200 K). An air ratio of 0.2–0.3 is most favourable for producing CO-rich gas. To produce hydrogen-rich gas at atmospheric pressure, the system should operate in the temperature range from 1100 to 1300 K and at an air ratio of 0.15–0.25.
- (4) Experimental evidence is provided demonstrating that real gasification processes deviate from chemical equilibrium. Any equilibrium-based model that does not account for such deviations is subject to error in predicting gas composition and overall efficiency. The pure equilibrium model is therefore modified to account for non-equilibrium factors. The concept of elemental availability is proposed, incorporating experimental results regarding unconverted carbon and methane.

- (5) The modified model predicts product gas compositions, product heating value, gas yield and cold gas efficiency in good agreement with experimental data. Further work is recommended to examine the role of tar, coke (containing hydrogen as well as carbon) and moisture in determining the final gas composition.

## Acknowledgements

The authors are grateful to Milaim Dervishaj and Dr. Yonghua Li for their assistance in the experimental study. Financial assistance from the Natural Sciences and Engineering Research Council of Canada is gratefully acknowledged. Use of the facilities of the Pulp and Paper Centre at UBC is also greatly appreciated.

## References

- [1] Schuster G, Loffler G, Weigl K, Hofnauer H. Biomass steam gasification—an extensive parametric modeling study. *Bioresource Technology* 2001;77:71–9.
- [2] Knoef HAM. Gasifier inventory, <http://www.btgworld.com/gi/>, 2002.
- [3] Beenackers AACM. Biomass gasification in moving beds, a review of European technologies. *Renewable Energy* 1999;16:1180–6.
- [4] Babu SP. Thermal gasification of biomass technology development: end of task report for 1992 to 1994. *Biomass and Bioenergy* 1995;9:5–15.
- [5] Ergudenler A, Ghaly AE. Quality of gas produced from wheat straw in a dual-distributor type fluidized bed gasifier. *Biomass and Bioenergy* 1992;3:419–30.
- [6] Caballero MA, Aznar MP, Gil J, Martin JA, Frances E, Corella J. Commercial steam reforming catalysts to improve biomass gasification with steam-oxygen mixtures. 1. Hot gas upgrading by the catalytic reactor. *Industrial and Engineering Chemistry Research* 1997;36:5227–39.
- [7] Corella J, Orio A, Aznar P. Biomass gasification with air in fluidized bed: reforming of the gas composition with commercial steam reforming catalysts. *Industrial and Engineering Chemistry Research* 1998;37:4617–24.
- [8] Liu P, Guo XF, Wu CZ, Chen Y, Arai N. Gasification characteristics of biomass wastes in fluidized bed gasifier. *Journal of Propulsion and Power* 2000;16:606–8.
- [9] Vamvuka D, Woodburn ET, Senior PR. Modeling of an entrained flow coal gasifier. 1. Development of the model and general predictions. *Fuel* 1995;74:1452–60.
- [10] Chen CX, Horio M, Kojima T. Numerical simulation of entrained flow coal gasifiers. Part I: modeling of coal gasification in an entrained flow gasifier. *Chemical Engineering Science* 2000;55:3861–74.
- [11] Fiaschi D, Micheleni M. A two-phase one-dimensional biomass gasification kinetics model. *Biomass and Bioenergy* 2001;21:121–32.
- [12] Chern SM, Walawender WP, Fan LT. Equilibrium modeling of a downdraft gasifier. 1. Overall gasifier. *Chemical Engineering Communications* 1991;108:243–65.
- [13] Ruggiero M, Manfrida G. An equilibrium model for biomass gasification processes. *Renewable Energy* 1999;16:1106–9.
- [14] Knoef HAM. The UNDP/World Bank monitoring program on small scale biomass gasifiers (BTG's experience on tar measurement). *Biomass and Bioenergy* 2000;18:39–54.
- [15] Gil J, Corella J, Aznar MP, Caballero MA. Biomass gasification in atmospheric and bubbling fluidized bed: effect of the type of gasifying agent on the product distribution. *Biomass and Bioenergy* 1999;17:389–403.
- [16] Brereton CMH, Grace JR, Yu J. Axial gas mixing in a circulating fluidized bed. In: Basu P, Large JF, editors. *Circulating fluidized bed technology II*. New York: Pergamon Press, 1988. p. 307–14.
- [17] Lide DR. *CRC Handbook of chemistry and physics*, 74th ed. Boca Raton, FL, USA: CRC Press, 1994.
- [18] van der Drift A, van Doorn J, Vermeulen JW. Ten residual biomass fuels for circulating fluidized-bed gasification. *Biomass and Bioenergy* 2001;20:45–56.
- [19] Li XT. Biomass gasification in a circulating fluidized bed. PhD Thesis, Department of Chemical and Biological Engineering, University of British Columbia, 2002.
- [20] Pan YG, Roca X, Velo E, Puigjaner L. Removal of tar by secondary air in fluidized bed gasification of residual biomass and coal. *Fuel* 1999;78:1703–9.
- [21] Moersch O, Spliethoff H, Hein KRG. Tar quantification with a new online analyzing method. *Biomass and Bioenergy* 2000;18:79–86.
- [22] Rapagna S, Jand N, Kiennemann A, Foscolo PU. Steam-gasification of biomass in a fluidized bed of olivine particles. *Biomass and Bioenergy* 2000;19:187–97.
- [23] Sutton D, Kelleher B, Ross JRH. Review of literature on catalysts for biomass gasification. *Fuel Processing Technology* 2001;73:155–73.
- [24] Hebden D, Stroud HF. Coal gasification processes. In: Elliott MA, editors. *Chemistry of coal utilization 2nd suppl.* vol. New York: Wiley, 1981, p. 1599–752.
- [25] Probststein RF, Hicks RW. *Synthetic fuels*. New York: McGraw Hill, 1982.
- [26] Smith WR, Missen RW. *Chemical reaction equilibrium analysis: theory and algorithms*. New York: Wiley, 1982.
- [27] White WB, Johnson SM, Dantzig GB. Chemical equilibrium in complex mixtures. *Journal of Chemical Physics* 1958;28:751–5.
- [28] Zeleznik FJ. Calculation of complex chemical equilibria. *Industrial and Engineering Chemistry* 1968;60:27–57.
- [29] Li XT, Grace JR, Watkinson AP, Lim CJ, Ergudenler AE. Equilibrium modeling of gasification: a free energy minimization approach and its application to a circulating fluidized bed coal gasifier. *Fuel* 2001;80:195–207.
- [30] Chase MW Jr, Davies CA, Downey DJ Jr, Frurip DJ, McDonald RA, Syverud AD, JANAF thermodynamic tables,

- 3rd ed. Journal of Physical and Chemistry References Data 1985;14:1–1856 (Suppl 1.).
- [31] Watkinson AP, Lucas JP, Lim CJ. A prediction of performance of commercial coal gasifiers. *Fuel* 1991;70: 519–27.
- [32] von Fredersdorff CG, Elliott MA. Coal gasification. In: Lowry HH, editor. *Chemistry of coal utilization*. New York: Wiley, 1963.
- [33] Coates RL, Chen CL, Pope BJ. Coal devolatilization in a low pressure, low residence time entrained flow reactor, in Coal gasification. In: Massey LG, editor. *Advances in chemistry series 131*. Washington DC: American Chemical Society, 1974, p. 92–107.
- [34] Grace JR, Li XT, Lim CJ. Equilibrium modelling of catalytic steam reforming of methane in membrane reactors with oxygen addition. *Catalysts Today* 2001;64:141–9.